Citation: Spittel D, Poppe J, Meerbach C et al (2018) Absolute Energy Level Positions in CdSe Nanostructures from Potential-Modulated Absorption Spectroscopy (EMAS). ACS Nano. 11(12): 12174-12184.

Absolute Energy Level Positions in CdSe-Nanostructures from Potential Modulated Absorption Spectroscopy (EMAS)

Daniel Spittel,[†] Jan Poppe,[†] Christian Meerbach,[†] Christoph Ziegler,[†] Stephen G. Hickey,[‡] and Alexander Eychmüller*[,†]

†*Physical Chemistry, Technische Universität Dresden, Bergstr. 66b, 01062 Dresden, Germany*

‡*School of Chemistry and Biosciences, University of Bradford, Bradford, BD7 1DP, Great Britain*

E-mail: Alexander.Eychmueller@chemie.tu-dresden.de
Phone: +49 351 463-39843. Fax: +49 351 463-37164

Abstract

Semiconductor nanostructures like CdSe quantum dots and colloidal nanoplatelets exhibit remarkable optical properties, making them interesting for applications in opto-electronics and photocatalysis. For both areas of application a detailed understanding of the electronic structure is essential to achieve highly efficient devices. The electronic structure can be probed using the fact that optical properties of semiconductor nanoparticles are found to be extremely sensitive to the presence of excess charges that can for instance be generated by means of an electrochemical charge transfer *via* an electrode. Here we present the use of potential modulated absorption spectroscopy (EMAS) as a versatile spectroelectrochemical method to obtain absolute band edge positions of CdSe nanostructures *versus* a well-defined reference electrode under ambient conditions. In this the spectral properties of the nanoparticles are monitored dependent on an applied electrochemical potential. We developed a bleaching model that yields the lowest electronic state in the conduction band of the nanostructures. A change in the band edge positions caused by quantum confinement is shown both for CdSe quantum dots as well as for colloidal nanoplatelets. In the case of CdSe quantum dots these findings are in good agreement with tight binding calculations. The method presented is not limited to CdSe nanostructures but can be used as a universal tool. Hence, this technique allows the determination of absolute band edge positions of a large variety of materials used in various applications.

Keywords: spectroelectrochemistry, semiconductor nanoparticles, band edge position, nanoplatelets, potential modulation, absorption

Important modern applications based on nanoparticles, such as: solar energy harvesting,[1–4] LED technology,[5–8] opto-electronics,[9,10] photocatalysis,[11,12] sensing[13–15] and bio-imaging[15,16] involve charge transfer processes between the nanoparticles and an adjacent phase. As a logical consequence of the increase in the band gap energy with decreasing particle

size the absolute energy positions of the valence band (VB) and conduction band (CB) shift and thus it is not only the magnitude of the band gap that one must consider.

The relative positions of the CB and VB in the nanoparticle with respect to those of the solution species have in turn a major impact on the charge transfer rates to the adjacent phase, *e.g.* the charge separation within a quantum dot sensitized solar cell (QDSSC) or the redox reactions happening at the surface of a nanoparticulate catalyst or electrochemical sensor. The knowledge concerning the absolute energy positions of the electronic states in semiconductor nanoparticles is therefore of crucial importance not only for fundamental research but also for many technological applications.

In contrast to the band gap energy, which can be determined by optical absorption spectroscopy, the measurement of the absolute energy positions of the electronic levels of a nanostructure like a quantum dot or a nanoplatelet, is far more challenging. In order to determine these absolute energy positions a variety of methods based on photoemission spectroscopy,[17–21] electrochemistry and photoelectrochemistry[22–24] have been developed.

However, some of these techniques are usually carried out in ultra high vacuum. In addition to the specific semiconductor material that the nanoparticles are composed of, the chemical environment in which the nanoparticles are located also has a major influence on their electronic structure and consequently the positions of the band edges. The influence of the immediate environment surrounding the particles is of particular importance from a technological point of view, as in many applications the semiconductor material is in direct contact with an electrolyte. Thus, for instance the band positions at the surface are altered by the presence of surface charges which arise from the adsorption and desorption of specific ions in the electrolyte.[23,25–27] Therefore, photoemission techniques are not suitable to probe the materials under "working" conditions, where such environmental influences must be considered. Moreover, it may be the case that due to the small density of states at the valence band edge of the semiconductor particles photoemission data might further be complicated[28] and beyond that these techniques require major technical efforts, elaborate sample preparation and are consequently expensive to implement.

Hence, a promising approach that may be used to determine the absolute positions of the band edges, is to probe the changes in the optical properties of the nanocrystals which develop during the electron transfer into the energy bands by spectroelectrochemical techniques. These methods are based on the Burstein-Moss effect, which describes the change in the absorption properties of a degenerate semiconductor. A semiconductor becomes degenerate when the doping densities are sufficiently high that the Fermi level is shifted into the majority carrier band. As the near edge states become populated by charge carriers, optical transitions into (or out of) these states become less probable and therefore a bleach of these transitions can be observed.

This effect can also be induced electrochemically by the application of a suitable potential to the material using a potentiostat which additionally offers the opportunity to measure the potential at which the electron injection occurs with respect to a known reference potential. It has been shown that this spectroelectrochemical approach can be used to study bulk semiconductors[29] as well as nanoparticulate systems.[30–33] Liu and Bard were the first to observe a reversible hypsochromic shift in the absorption onset of CdS nanoparticles immobilized on transparent conductive electrodes at reductive potentials.[29] Later, in the course of the development of dye sensitized solar cells this effect was also shown for electrodes coated with porous films of TiO_2[31,34–36] and ZnO.[37] In addition to the hypsochromic shift a corresponding nearly reversible electrochemical current response was observed, allowing the measurement of the charge injected into the nanoparticlulate film to be made.

Wang and co-workers studied the electrochemical bleaching of the first transition of dropcast CdSe nanocrystals on platinum or gold working electrodes.[38] Nanocrystals of different sizes were investigated and the size dependence of the po-

tential at which the bleach could be found was observed. Electrochemically induced bleaching was later studied on compact films of CdSe[30,39] and PbSe[40,41] nanoparticles by Guyot-Sionnest and co-workers as well as more recently also heterojunctions of PbSe and CdSe[42] by Boehme and co-workers. The observed potential dependent bleach of the fundamental absorption edge correlates with a strongly increased conductivity of the films as the lowest conduction band states become populated by electrons.

Araci *et al.* studied charge injection processes of a sub-monolayer of CdSe-nanoparticles using the technique of attenuated total reflectance (ATR). Frequency modulation of the applied potential was employed to determine the rate of electron injection with respect to the dependence of the linker employed to attach the nanoparticles.[43]

Hickey and Riley introduced EMAS to study the bleaching of sub-monolayers of CdS nanoparticles on indium tin oxide (ITO).[44] In this work potential modulation and lock-in detection were applied by which the sensitivity with respect to the determination of changes in the absorption is greatly enchanced. However, the polydispersivity of the materials investigated did not allow a detailed spectroscopic characterization of the quantum confined semiconductor particles. Up to now the utilization of the electrochemically induced Burstein-Moss effect in order to examine the electronic structure of semiconductor nanoparticles on an absolute energy scale and especially its size dependence has received just little attention.

In the following report the concept of EMAS is applied to semiconducting nanostructures. The decision to use CdSe as the semiconductor material was mainly motivated by the fact that it is a widely investigated material. In general, there are few limitations to the semiconductor materials employed and it is possible to probe a wide variety of other semiconductors. To evaluate the influence of dimensionality a comparison to nanoplatelets is added. Some significant differences are given here but the theoretical description of EMAS as applied to two dimensional nanostructures is beyond the scope of this work and will be a subject of further papers.

Results and Discussion

Measuring Principle and Model for the Bleaching Observed in EMAS

The Fermi level of a certain phase is per definition equal to the electrochemical potential of the electrons within that phase.[45,46] Upon contact, which is established during the nanoparticle deposition step, the initial Fermi levels of the electrode and the nanoparticles are assumed to have equalize through charge transfer. The Fermi level of such a system can be measured and also adjusted by the application of a potential with respect to a defined reference electrode by means of a potentiostat (Figure 1 a). This means that by controlling the potential of the electrode the Fermi level of the particle can in effect be adjusted to a desired value.

Below the conduction band edge no charge flow is expected in a perfect crystalline semiconductor as there are no electronic states in the band gap region (Figure 1 b1) and therefore the change in absorption is also expected to be zero (Figure 1 b2). In the proximity of the absorption edge the absorption profile of semiconductor nanocrystals is determined by the presence of distinct exciton states which are each composed of a discrete electron state in the conduction band and a discrete hole state in the valence band. Under such conditions the application of a potential which is more negative than that of the conduction band edge of the nanoparticles results in the population of the now available electronic states.

The lowest electron level in spherical CdSe quantum dots is the $1S_e$ state[47] and when this is populated, all excitonic transitions that promote electrons into that state become bleached (Figure 1 c1) which is indicated by a change in absorption (Figure 1 c2). Since the occupation probability of the electrons in the electrode is distributed according to Fermi-Dirac statistics the transitions into the $1S_e$ state are not instantaneously "switched off" as the Fermi level

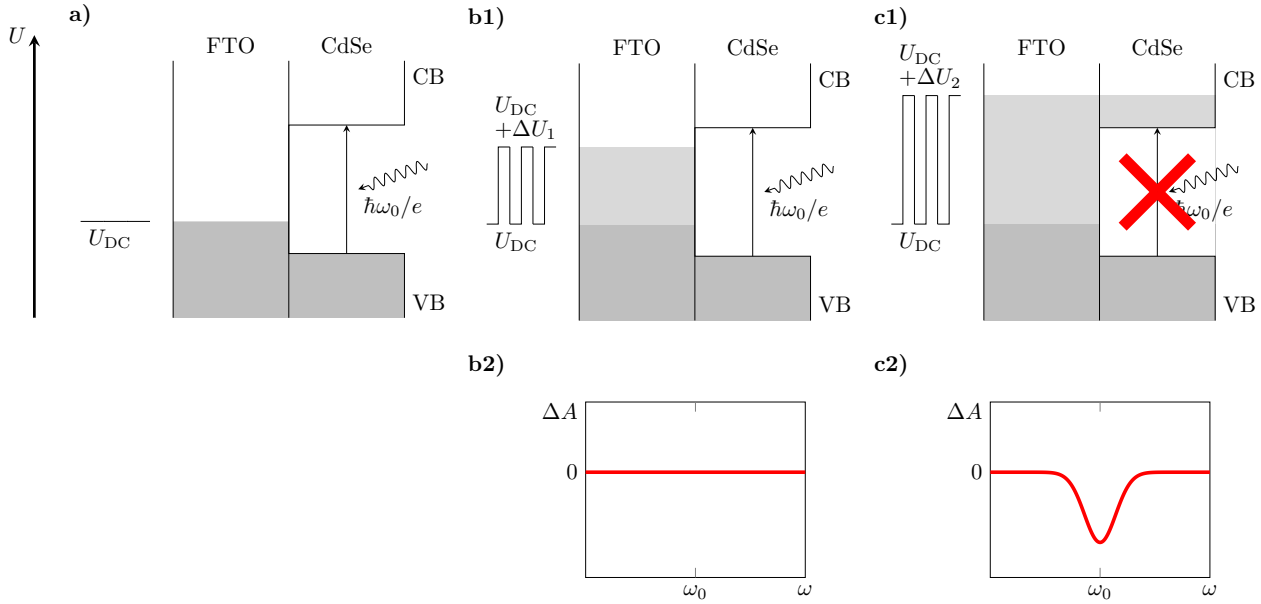

Figure 1: *Measuring principle of the EMAS technique. A constant potential within the bandgap of a semiconductor nanoparticle U_{DC} is applied (a). Then a periodic square wave potential with the amplitude ΔU_i is added to U_{DC} (b1). At this point the maximum of the potential does not reach the lower conduction band edge, so no change in absorbance is expected (b2). The amplitude is now varied in e.g.* 50 mV *steps and for every step a spectrum between* 350 nm *and* 800 nm *is recorded. At a certain point the fundamental absorption of the semiconductor is quenched because of the occupation of the lowest conduction band states (c1). This change in absorbance (c2) is calculated and finally plotted against the corresponding potential applied (Fig. 3 and 6 top left).*
The reader will want to be aware that all E_i symbols refer to energy values whereas U_i symbols describe the corresponding potential values.

equals the state's energy, but rather are gradually bleached at finite temperatures.
The onset of the bleach response is expected when the Fermi level of the electrode is located at approximately 4 k_BT ($\approx$ 100 meV at room temperature) below the lowest conduction band state energy (the occupancy of this state is therefore 0.01). As the electrode Fermi level approaches the band edge states* the occupation probability should be 0.5, as per definition. Thus, the probability that the lowest electron state of the CdSe nanoparticles deposited onto the electrode is populated amounts to 50 % and therefore the absorption bands corresponding to the respective exciton transition are expected to decrease to 50 % of the initial intensity. The main assumption on this occasion is the proportionality between the occupation of the electronic states which correspond to the most intensive absorption peaks and the change in absorption intensity.
When the Fermi level is located 4 k_BT above the band edge states the absorption bands should completely vanish (occupation probability = 0.99). Ideally, the potential dependent bleach intensity should therefore follow a sigmoid curve progression which corresponds to the Fermi-Dirac distribution. However, the deposited "real" nanoparticles introduce an ensemble of $1S_e$ states in the case of quantum dots and a broadening of the band edge in the case of platelets. Consequently the curve that one obtains is expected to be somewhat broader than the Fermi-Dirac distribution function. We have assumed a symmetrical energy distribution of the $1S_e$ state and a symmetrical broadening of the band edge in the platelets, so the broadening has no influence on the position of the inflection

*For spherical quantum dots the $1S_e$ state is meant which is a discrete electronic state. For platelets, however, the conduction band begins with a quasi continuous band, so the first states within this band are meant.

point, *i.e.* where the Fermi level is equal to the mean energy of the state.

Based on these observations a model function to describe the potential dependent bleach signal intensity can be derived:

$$\Delta A(U) = \frac{\Delta A_1 - \Delta A_2}{1 + \exp((U - U_0)/\xi)} + \Delta A_2 \quad (1)$$

where $\Delta A(U)$ is the measured potential dependent change in absorbance, U is the applied potential with respect to a reference electrode, U_0 refers to the potential where the change in absorbance equals 50 % of the total change in absorbance and indicates the inflection point of the curve, ξ is a measure of the spread of the sigmoidal profile, ΔA_1 and ΔA_2 are the asymptotically approached values for the change in absorbance far from U_0. The model function essentially corresponds to the Fermi-Dirac distribution, but accounts for the changes in absorbance as measured for the state's occupancy and for the broadening due to its energy dispersion.

The most important parameter obtained from this model is U_0 which corresponds to the electrochemical potential of the lowest conduction band state with respect to a well defined reference electrode potential.

For a detailed block diagram and a list of typical measurement parameters which are used in the experiments below, see the supporting information (Figure and Table S1).

Application to CdSe-Nanoparticle Sub-Monolayers

Sub-monolayers of CdSe nanocrystals have been prepared on fluorine doped tin oxide (FTO) substrates according to the methods presented in the supporting information. While using submonolayers coulomb interaction between the attached nanoparticles is thought to be avoided and a better access of electrolyte molecules to the particles is provided, thus incomplete or hindered diffusion of cations through a nanoparticle layer can be excluded. Figure 2 a) shows a set of EMAS difference spectra for such an FTO electrode covered with 4.9 nm quantum dots in the range between 350 and 800 nm. The corresponding absorption spectra of the particle layer and the respective colloidal solution are shown in Figure 2 2b) for comparison.

While sum of the DC potential (U_{DC}) and modulated potential (ΔU_{i}) applied to the interface is below −1.0 V vs. Ag/AgCl no significant changes in the spectral profiles are obtained, but upon increasing the potential to more negative values drastic changes in the differential absorption of the sample can be observed. The four significant bleach bands **A** - **D** observed in the EMAS spectra at 606 nm, 578 nm, 525 nm and 499 nm are in exact agreement with the first four optical transitions observed in the absorption spectrum. A fifth much weaker bleach signal **E** is observed at 455 nm and is assumed to be correlated with an additional transition, which is barely visible in the absorption spectrum, but more pronounced in its second derivative. A further bleach band is observed in the UV region at approximately 360 nm. Moreover, features associated with induced absorption effects are observed in the EMAS spectra. A proportionally intense induced absorption band (**X**) is obtained at 552 nm between bleach bands **B** and **C**, which cannot be assigned to a transition in the absorption spectrum. Between the induced absorption **X** and the signals **B** and **C** two isosbestic points are obtained, one at 534 nm and the other at 565 nm. Another broad induced absorption occurs at wavelengths above 650 nm.

In order to identify artifacts caused by the electrode, the measurements were also conducted on blank FTO substrates.

The respective EMAS spectra and the absorption spectrum of the blanks are shown in Figure 2 c) and d). The comparison with Figure 2 a) reveals that the bleach signal centered at 360 nm and the induced absorption band towards the far red observed in the EMAS spectra of the particle modified electrode can be clearly attributed to the FTO as these features exactly resemble features observed in the blank spectra. It is most likely that the bleach band at 360 nm is related to the absorption edge of FTO, which is reported to lie in the range of 390 – 340 nm depending on the doping level.[48] The induced absorption is caused by excitation of

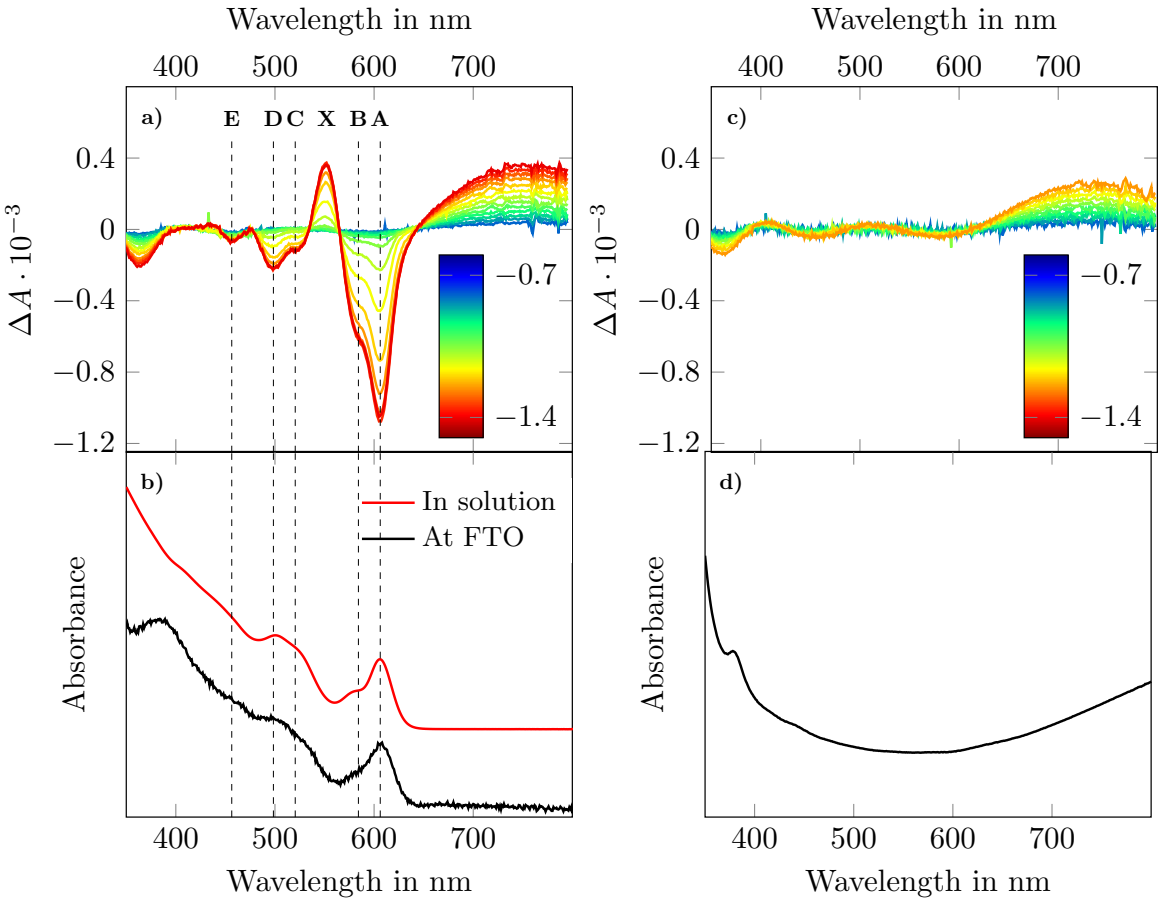

Figure 2: *a) EMAS spectra of submonolayers of CdSe nanocrystals deposited on FTO, plotted as a change in absorbance. Negative (positive) peaks represent bleaches (induced absorptions). The FTO electrode is under potentiostatic control and held at* $U_{DC} = -0.7\,\mathrm{V}$ *vs. Ag/AgCl. Additionally a square-wave modulation is superimposed (*$f = 67\,\mathrm{Hz}$*,* ΔU *is consecutively increased from* $0.1\,\mathrm{V}$ *up to* $0.6\,\mathrm{V}$ *to yield the stated value in the legend). b) The corresponding absorption spectra of the particle film on FTO (black) and the colloidal solution (red). c) EMAS spectra of a blank FTO substrate and d) the corresponding absorption spectrum.*
The color bar represents the potential (maximal amplitude of the applied square wave plus DC-potential) vs. the reference electrode (Ag/AgCl 3M NaCl) by which every single difference spectrum war recorded.

free electrons in the conduction band of FTO, as their concentration increases as the potential is set to progressively more negative values. The occurrence of intraband absorptions associated with the deposited nanoparticles is not expected in that wavelength range as transitions promoting electrons from the $1S_e$ states to higher conduction band states usually occur above 2500 nm.[49–51] The low intensity undulating features between 400 and 600 nm observed in Figure 2 c) may be attributed to interference effects caused by the FTO thin film as its dielectric properties are expected to slightly change upon potential modulation.

While the observed features are likely to be attributed to band filling, such kinds of changes in the fundamental absorption of semiconductors can also be induced by the presence of an electric field. An electrochemical interface generally features a steep potential drop across the phase boundary. Depending on the electrolyte concentration, the potential drops across a distance of only a few Åon the solution side of the interface.[45] Consequently, the electrical field strength adjacent to the electrode surface is considerably high and hence influences on the optical prop-

erties of the quantum dots caused by the field have to be taken into account. Two effects could be envisaged to occur under these conditions, namely the Stark effect, which is mainly characterized by a splitting of degenerate energy levels, and the Franz-Keldysh effect which is characterized by an apparent broadening in the optical band gap energy.

The Franz-Keldysh effect is a bulk semiconductor phenomenon, as it is based on the concept of spatially continuous bands and therefore should not play a role in the present case. By contrast, Stark effects are known to occur in semiconductor nanocrystals.[52–55] Depending on their relative orientation the interaction between the external electric field and the dipole of the excited state can either decrease or increase the energy of that state. Due to the size distribution present within the particle ensemble this leads to a broadening of the individual transitions and should therefore induce a narrow absorption band located to the low energy side of the fundamental absorption.[55] Evidence for the presence of such effects in the data is not observed and therefore the modulation of the electric field across the electrochemical double layer does not appear to influence the measurements. In order to entirely exclude artifacts caused by this issue another set of EMAS spectra have been recorded, under the application of a DC potential of 0 V instead of −0.7 V *versus* the Ag/AgCl reference. The onset potential of the bleach associated with transition **A** as well as the curve profile for the potential dependent intensity are in excellent agreement with those obtained for −0.7 V. These findings confirm the hypothesis stated above, and thus the features observed in the EMAS spectra can be assigned to band filling with greater certainty.

For the first transition, an additional plot of $\Delta A/A$ *vs.* U is provided in the supporting information (Figure S5). According to the model, the onset potential of the bleach at −1 V with respect to the reference electrode refers to the situation where the Fermi level is located roughly 4 k_BT below the $1S_e$ states of the largest particles within the size distribution. As the Fermi level is further shifted towards more negative potentials the probability that electrons will be transferred across the electrode/nanoparticle interface and populate free $1S_e$ states increases. Additionally the smaller sized fraction within the particle ensemble is progressively affected. As a result optically excited electronic transitions into the $1S_e$ states from the valance band states become less probable leading to a bleach of the respective absorption bands.

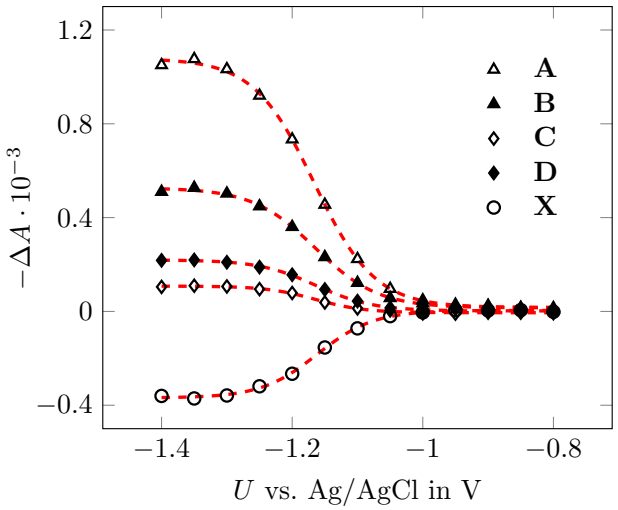

Figure 3: *Plot of the bleach signal intensity of the transitions **A** - **D** and the induced absorption band **X** with respect to the applied potential. The dashed lines represent fits according to the model presented above.*

According to the literature, the two transitions **A** and **B** can be assigned to the $1S_{3/2}$ - $1S_e$ and $2S_{3/2}$ - $1S_e$, respectively.[56,57] With regard to the bands **C** and **D**, there are different opinions as to whether these are best assigned to the $1S_{1/2}$ - $1S_e$ (**C**) and the $2S_{1/2}$ - $1S_e$ (**D**)[56,57] or the $1P_{3/2}$ - $1P_e$ (**C**) and $1S_{1/2}$ - $1S_e$ (**D**) transition.[24,30,39,58,59] The analysis of the potential dependence of the respective bleach signatures may shed some further light on this issue.

Figure 3 shows the potential dependent change in absorbance for the transitions **A** - **D** and induced absorption **X** at the wavelengths of the respective maximal intensities. As expected the measured data follow a sigmoid curve progression for each band, whereby the change in absorbance sets in at −1.05 V and reaches a plateau above −1.3 V. The obtained data were fitted according to equation 1 presented above with the optimized fitting parameters summa-

Table 1: *Optimized parameter sets obtained by fitting the potential dependent intensities of the bands A - D and X determined by EMAS of 4.9 nm CdSe particles according to equation 1. The bands were assigned to the respective exciton states according to Norris et al.*[56]

Band	Assigned transition	U_0 vs. Ag/AgCl in V	ξ in mV	$\Delta A_1 \cdot 10^{-4}$	$\Delta A_2 \cdot 10^{-4}$
A	$1S_{3/2} - 1S_e$	−1.166	42	−10.82	−0.17
B	$2S_{3/2} - 1S_e$	−1.165	45	−5.37	−0.16
C	$1S_{1/2} - 1S_e$	−1.164	38	−1.08	0.06
D	$2S_{1/2} - 1S_e$	−1.163	44	−2.19	−0.02
X		−1.162	42	3.69	−0.06

rized in Table 1.

For the sigmoid inflection point (U_0) almost equal values were determined for all signals. Furthermore the obtained ξ parameters, which defines the widths of the sigmoid curves, are in agreement with the theoretically predicted value for a Gaussian-like density of states function, which is distributed by 40 meV. These findings therefore imply that the bleached transitions are due to the attenuated promotion of electrons from different states in the valence band to the same final state in the conduction band which is located at −1.164 V vs. Ag/AgCl. As the fundamental transition (transition **A**) is bleached, the electronic state, which is populated during the experiment can be explicitly assigned to the lowest conduction band state, which is the $1S_e$ state. As the populated state can now be identified with a high degree of certainty the bleached transitions can be more clearly assigned to the following exciton states: $1S_{3/2}$ - $1S_e$ (**A**), $2S_{3/2}$ - $1S_e$ (**B**), $1S_{1/2}$ - $1S_e$ (**C**), $2S_{1/2}$ - $1S_e$ (**D**), which is in agreement with theoretical calculations and pump-probe spectroscopy experiments.[56]

In Figure 3 the evolution of the induced absorption signal **X** is also shown. It turns out that the inflection point of the establishing band is identical to those obtained for the bleached transitions. Consequently, the induced absorbance is directly connected to the population of the $1S_e$ state. Hence, it can be assumed that band **X** at 550 nm corresponds to the absorption of the CdSe particles in their exited states and may result from Coulomb interactions of the injected charge with the optically excited electron-hole pair leading to changes in the selection rules and an increase in the transition probability of initially forbidden transitions.[56,60]

The existence of the isosbestic points at 534 and 565 nm in the EMAS spectra furthermore indicates that only two species are involved during the observed bleaching process. The two species, which are the initially uncharged nanocrystals and the nanocrystals with an occupied $1S_e$ state, differ in their individual absorption spectra. The isosbestic points occur because the two species absorb light at these two specific wavelengths to the same extent, and the amount of particles attached to the electrode remains constant during the experiment.[61] Consequently, in the modulation spectrum the change in absorbance is zero at these wavelengths, independent of the applied electrode potential. The ratio at which both species are present is dictated by the Fermi-Dirac distribution. Interestingly energy distribution of the $1S_e$ state appears to be narrow enough that the isosbestic points do not result in a smearing out of the crossover point. The occurrence of the isosbestic points illustrates the presence of distinct, energetically separated electronic states as are typically observed for quantum-confined electronic structures.

Since the electrochemical potential of the $1S_e$ state has been determined, the potential positions of the electronic states within the upper portion of the valence band can now be obtained from the respective transition energies obtained from the EMAS spectra. However, a simple addition of the optical energies associated with the potential of the $1S_e$ states is not valid, as the corresponding bands are not associated with interband transitions, but rather with excitonic

transitions. Therefore the exciton binding energy, *i.e.* the Coulomb interaction between the electron and hole needs to be considered in accordance with the following equation:

$$U_{\mathrm{g}} = U_{\mathrm{g,opt}} + \frac{1.8e}{4\pi\varepsilon_{\mathrm{r}}^{\infty}\varepsilon_0 r} \quad (2)$$

With U_{g} being the potential difference between the valence and the conduction band, $U_{\mathrm{g,opt}}$ the potential value which is estimable by optical spectroscopy, e the elementary charge, $\varepsilon_{\mathrm{r}}^{\infty}$ the medium's relative permittivity at high frequencies, ε_0 the vacuum permittivity and r the radius of the spherical particle. Hence, for the potential of the individual valence band state $U_{\mathrm{S_h}}$ *versus* the reference the following applies:

$$U_{\mathrm{S_h}} = U_0 + \frac{\Delta E_{\mathrm{opt}}\left(\mathrm{S_h} - 1\mathrm{S_e}\right)}{e} + \frac{1.8e}{4\pi\varepsilon_r^{\infty}\varepsilon_0 r} \quad (3)$$

Here, U_0 is the electrochemical potential of the $1S_{\mathrm{e}}$ state as determined by EMAS and $\Delta E_{\mathrm{opt}}\left(\mathrm{S_h} - 1\mathrm{S_e}\right)$ is the energy of the transition between the respective valence band state and the $1S_{\mathrm{e}}$ state. The resulting electronic structure is sketched in figure 4. Except the very small signal at 455 nm no additional bleach signals were observed in the wavelength range below 500 nm. Thus transitions to higher electron states are not bleached under the experimental conditions employed here. The trivial reason for this finding could be that the Fermi level of the electrode is still too positive to populate these states. According to theory the next higher electronic state in the conduction band of CdSe nanocrystals is the $1P_{\mathrm{e}}$ state. IR spectroscopic investigations of chemically charged CdSe nanocrystals of comparable size reveal an induced absorption band in the mid infrared at roughly $3000\,\mathrm{cm}^{-1}$ referred to as a $1S_{\mathrm{e}}$ - $1P_{\mathrm{e}}$ intraband transition.[30] Consequently the $1P_{\mathrm{e}}$ state is estimated to be located around 0.4 eV more negative than the $1S_{\mathrm{e}}$ state. The onset of the bleaching of the respective optical transitions into the $1P_{\mathrm{e}}$ state should therefore not occur at applied potentials below −1.4 V vs. the Ag/AgCl reference electrode, again assuming an energy dispersion of 40 meV for that state. However, due to the emerging hydrogen evolution the application of potentials more negative than −1.4 V is accompanied with the appearance of additional artifacts associated with solvent decomposition.

Nevertheless $1P_{\mathrm{e}}$-filling was observed by other groups.[24,30,39] They use organic solvents like N,N-dimethylformamide or acetonitrile. We did measurements in acetonitrile too but we were not able to reproduce their findings. Except shifts of the band edge potentials affecting all transitions in the same manner, we could not find discrepancies in the inflection points.

Size Dependence

As has been demonstrated, the change in absorption reacts very sensitively to changes in potential, especially for the first transition. Therefore, EMAS is a powerful tool to accurately determine the absolute energy position of the $1S_{\mathrm{e}}$ state, *i.e.* the dependence of the conduction band edge position with respect to the particle diameter. For these investigations multilayers of CdSe nanoparticles in the size range between 2.4 and 5.9 nm have been prepared and attached to FTO electrodes.

The EMAS spectra of all samples show a bleach of the first four optical transitions and the appearance of the induced absorption band between transition **B** and **C**, with the exception of the spectrum of smallest sized sample which is essentially due to its weak signal-to-noise ratio. For the particle sizes 3.8, 3.4 and 2.9 nm an additional second induced absorption feature is observed at shorter wavelengths next to transition **D**. (See supporting information Figure S5 and S6).

With decreasing particle size, a rapid drop in the signal magnitude is observed. In comparison to the sample with the largest particle diameter, the magnitude of the bleach observed for the sample with the smallest particle diameter is two orders of magnitude smaller. Assuming that the absorption coefficient is directly proportional to the particle volume the decrease in signal intensity from the largest size (5.9 nm) to the smallest size (2.4 nm) is expected to amount to only approximately 7 %.

The lower intensities observed for the small particles are attributed to the less efficient adsorption

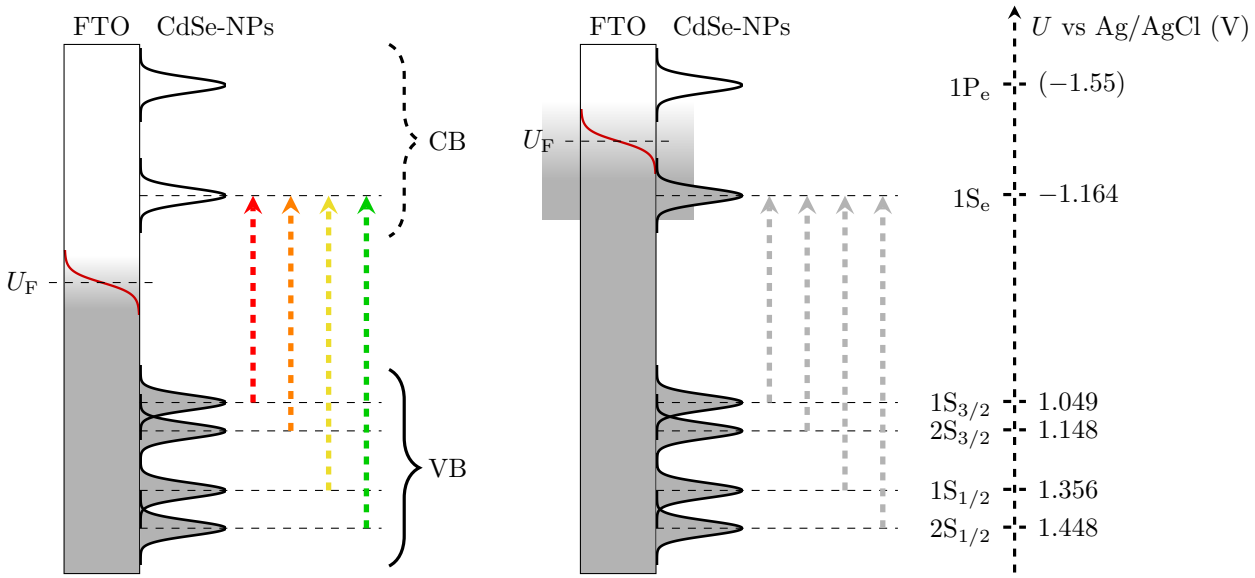

Figure 4: *Schematic of the transitions bleached via the population of the conduction band* $1S_e$ *state and the calculated potential positions of the individual electronic states within the bands versus the Ag/AgCl reference electrode. The valence band states have been calculated on the basis of the potential determined for the* $1S_e$ *state according to equation 3. The potential of the* $1P_e$ *state is estimated on the basis of results published by Guyot-Sionnest and coworkers.*[30] U_F *denotes the Fermi potential (corresponding to the Fermi energy).*

abilities of the smaller particle sizes during the deposition procedure and can be explained in terms of a much smaller radius and hence a more strongly curved surface. Hence, the interaction with multiple binding sites is less likely with the consequence that small particles are more prone to detach.

The respective plots of the bleach signal intensity *versus* the applied potential clearly reveal a shift of the sigmoid curve trace to more negative potentials with decreasing particle diameter and therefore increasing band gap energy. This finding is in agreement with the presence of the quantum confinement effect.

In order to determine the size dependent potential of the $1S_e$ state, which corresponds to the conduction band edge, the measured data were fit according to the model presented above. To reduce the influence of random errors the positions of the inflection points have been determined by averaging the results of at least five measurements at different sites on the electrodes.

Theoretically, it should be possible to determine the position of the valence band in similar fashion by applying the potential modulation across the valence band edge. However, the expected potential range for the valence band edge is located beyond the oxidation potential of water. Therefore, the valence band edge positions have been determined according to equation 3 by adding the optical band gap energy and the respective Coulombic interaction term to the conduction band level. The size dependent absolute energy levels of the conduction band and valence band are shown in Figure 5. Additionally the predicted dependencies based on theoretical calculations, namely the effective mass approximation (EMA) and a tight binding approach (TB), are shown for comparison.

In agreement with the quantum size effect, the determined band edge levels of the conduction band and valence band show a significantly convergent behavior with increasing nanocrystal diameter, which fits quite well with the theoretically predicted curves. The size dependence of the shifts of both band edges is found to be nearly equal. This is rather unexpected considering the fact that the band edge shifts should be related reciprocally to the respective charge carrier effective mass[62] and therefore a somewhat larger shift is expected for the conduction

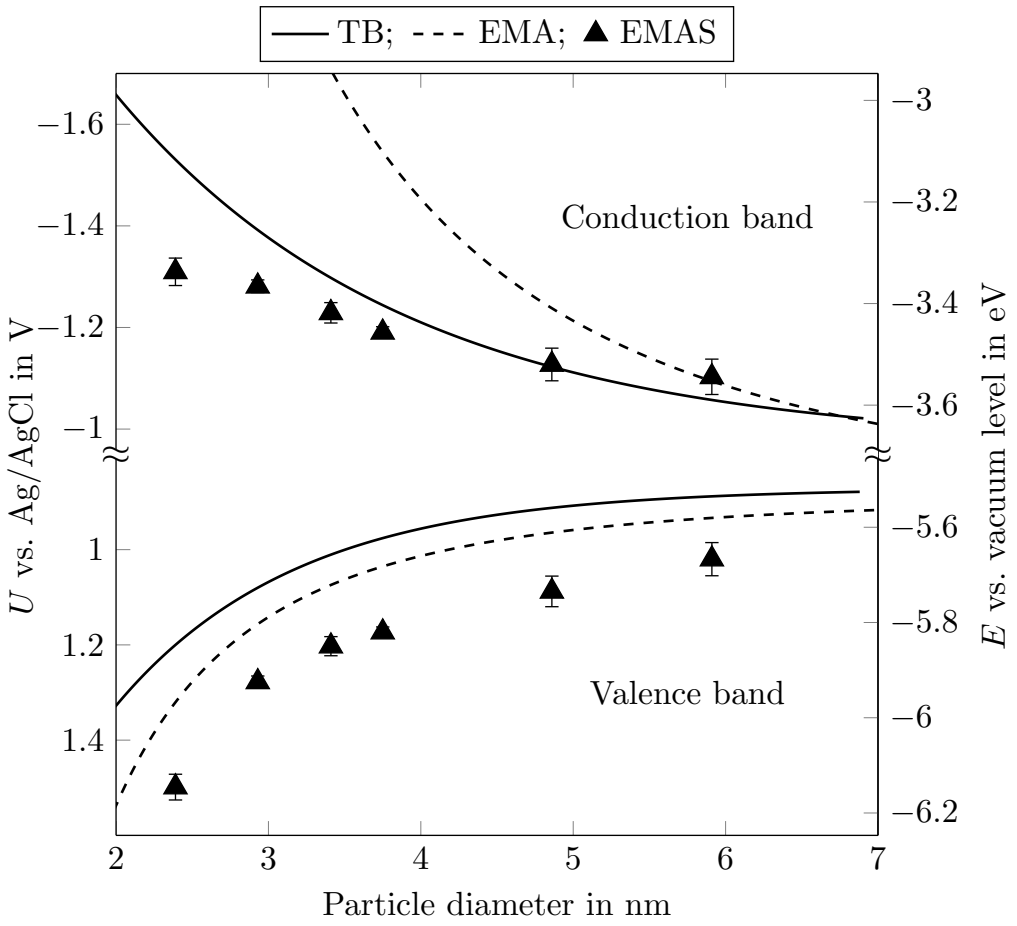

Figure 5: *Size dependence of the absolute energies of the conduction band edges and valence band edges for the set of CdSe nanocrystals determined by EMAS. Theoretically predicted curves based on the effective mass approximation (EMA) and a tight binding approach (TB) reported by Sapra and Sarma.[62] have been plotted for comparison. Whereas the size dependent band edges calculated by the tight binding approach closely match the measured data, the effective mass approximation increasingly overestimates the band gap for decreasing particle size, due to the assumption of that the respective charge carriers are confined by infinite energy barriers. Please notice the axis break at the potential/energy axis.*

band edge which is also expressed in the theoretically calculated curves. The observed loss in signal magnitude at potentials more negative than −1.3 V could provide a possible explanation for this effect. The detachment of particles from the electrode surface leads to a premature decrease in the bleach intensity before the potentials at which the signal intensity should reach the plateau are probed, *i.e.* as the occupation probability becomes one. Subsequently, the expected sigmoidal curve progression becomes distorted such that the inflection point corresponding to U_0 is slightly displaced towards more positive potentials.

Moreover, it follows that this effect is more pronounced for smaller particle sizes, as with decreasing particle size the bleach is observed at more negative potentials. If this artefact is taken into account, the measured data very closely resembles the curve progression predicted by the TB approach. On the other hand, the effective mass approximation reveals a much stronger dependence of the bandgap with size as obtained from EMAS. This is mainly due to the fact that in this model the confining potentials have been assumed to be infinite, leading to an overestimation of the confinement energy, especially for smaller crystal sizes. Furthermore, in the case of II – VI semiconductors the simple effective mass approximation does not account for the splitting

of the valence band into subbands.[62–66] TB calculations provide a substantial improvement in accuracy since it describes properties in terms of chemical bonds and therefore gives the model a more realistic physical base.[67] Sapra and Sarma have computed the size dependent shifts of the individual band edges for various II - VI semiconductor NCs by using a $sp^3\,d^5$-orbital based TB approach.[62]

To not exceed the scope of this paper, we will not discuss influences of other solvents like acetonitrile or methanol. But we did this investigation and the reader should be aware that changing the solvent of the electrolyte strongly affects and shifts the position of the estimated electronic states.

Also the cation of the electrolyte may influence the energetic positions because of intercalation processes that lead to Na-Se bonds within the particle.[68] This will introduce mid-gap states which then lead to undesirable charging before reaching the conduction band states. Also different capabilities of charge compensation, whether big cations are used or small ones, may affect the charging process, because of differences in the mobility or charge density of the ions.[69] The last point that should be mentioned is the problem of surface trapping. Until now there is no systematic investigation of this point with EMAS but we want to state that spherical particles varying their diameters and platelets varying their thicknesses and lateral sizes may be influenced all in a different manner by charging of local states.

Comparability of EMAS results, thus, is only given if usage of the same environment which implies electrolyte, working electrode material, temperature and the cleanliness of all compartments is ensured.

Application to CdSe-Nanoplatelets

The electronic structure of nanoplatelets differs completely from that of spherical nanoparticles. The density of states (DOS) in two dimensional electron gases is constant, which leads to a staircase structure in quasi two-dimensional quantum wells. Contrary to small spherical nanoparticles there are now quasicontinuous bands present and therefore many more electronic conduction band states which can be filled during the application of EMAS.

Furthermore, platelets have a much higher surface/volume ratio that potentially leads to more surface states. Those surface states can be filled during EMAS and provide a negative excess charge at the surface of the particles. It is therefore interesting to extend the powerful measuring technique from geometric nearly isotropic structures to those with strong geometric anisotropy. The simple model applied to nanoparticles is also applied to platelets. In Figure 6 top left, EMAS difference spectra are shown with linear absorption spectra of the nanoplatelet solution and of the coated substrate also provided for comparison. The difference spectra show three separated bleaching peaks. The spectral position of the bleaching peaks and the transition peaks in the linear absorption spectra are in excellent agreement which is highlighted by the dashed lines in Figure 6 left, where an assignment (denoted as **A**, **B** and **C**) for the peaks has been made. There is also a fourth smaller absorption between **B** and **C** which originates from a nanoplatelet fraction containing thinner platelets which were not completely removed during the purification process. Transitions **A** and **B** originate from the formation of 1S excitons, where the exited electron comes from the heavy-hole band and from the light-hole band, respectively.[70] *1S* denotes the exciton in the ground-state below its particular band edge. Higher excitations are possible but for all inter-band transitions the parity of the electron and hole wave function must not change. For transition **A** the corresponding exciton can be noted 1S-hh1-e1 indicating that the electron is excited in the first electron sub-band (in the conduction band) and the hole remains in the first sub-band of the hh band (in the valence band). Analogously the exiton, which is assigned to **B**, can be written as 1S-lh1-e1.

The appearance of induced absorption at both sides of the quenching peak indicates a potential induced broadening of the absorption. The reason for this is the electric field that is applied during the measurement process. Similar difference spectra were obtained by Achtstein et.

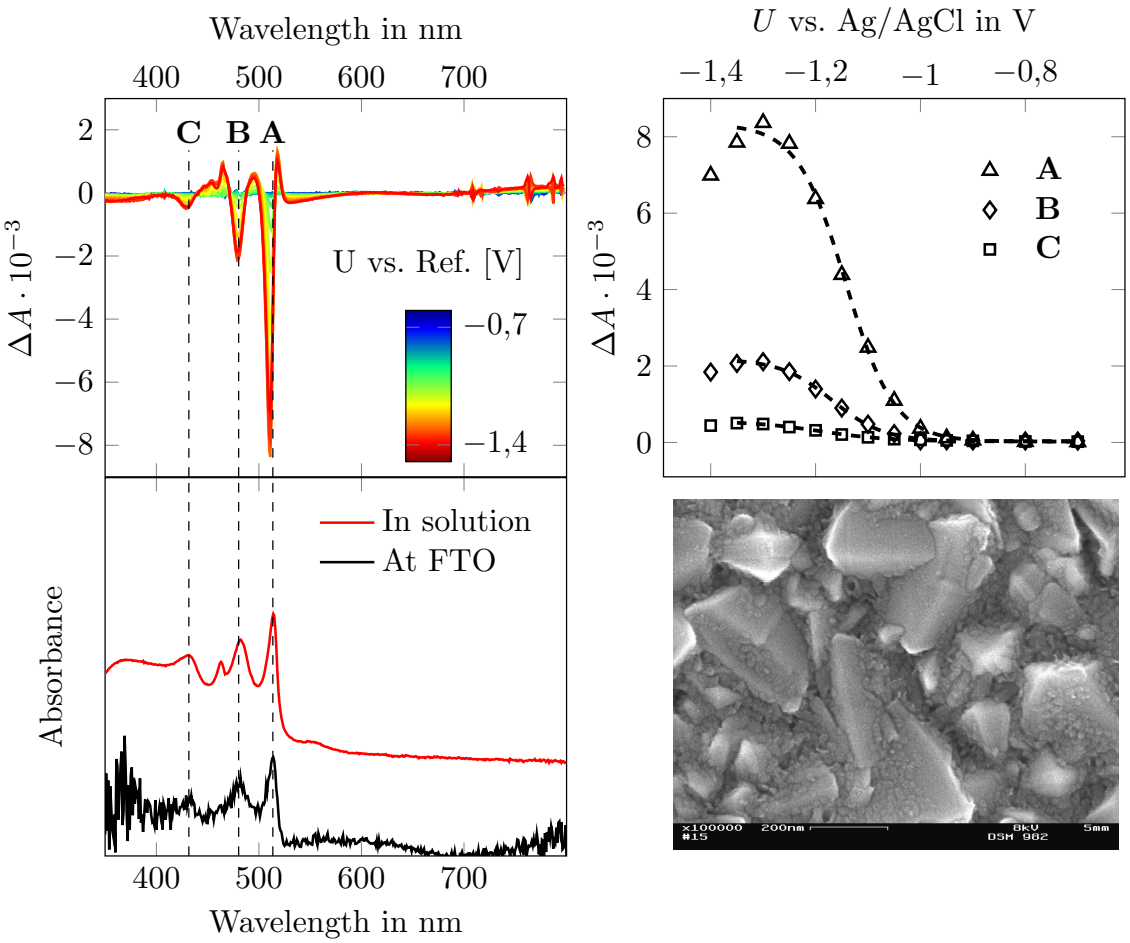

Figure 6: *top left: difference spectra obtained from an EMAS measurement. Every graph represents a applied potential amplitude which is displayed versus the Ag/AgCl reference electrode (Ag/AgCl/ 3M NaCl, $U_{ref} = 0,209$ V vs NHE). bottom left: linear absorption spectra of the nanoplatelet solution and of the coated FTO-Substrates. top right: change of absorption dependent on the applied potential amplitude. As dashed line, the fitted sigmoidal curve is drawn. bottom right: SEM image of the coated FTO-substrate.*

al.[71] where nanoparticles were fixed in a polymer matrix between two capacitor plates and a constant potential applied to the particles. Due to the quantum confined Stark effect (QCSE) and the quantum confined Franz-Keldysh effect (QCFKE) a broadening of the absorption curve was received and at the same time a loss in signal intensity. Both signal quenching and induced absorption occur to approximately the same extent which is different from the spectra presented here. These findings confirm the explanation that the bleaching observed is mainly due to occupation of electronic states and the induced absorption due to broadening because of the external electric field. On the other hand induced absorption could also originate from a changing of the exciton energy as a result of charging the nanostructure. However this can only explain the induced absorption signal at higher energy than the fundamental absorption in the uncharged case.

The EMAS spectra show a significant change in absorbance above 1 V in the cathodic direction *versus* the Ag/AgCl reference electrode. As was presented above the extent of the change in absorbance is plotted against the corresponding maximum potential which was applied during the measurement. After fitting the data to equation 1 the inflection point (U_0) amongst the other parameters, as listed in Table 2, were

Table 2: *Parameters extracted out of the $\Delta A - U$ plot. The standard deviation is given in brackets after the respective values.*

Transition	$\Delta A_1 \cdot 10^{-4}$	$\Delta A_2 \cdot 10^{-4}$	U_0 vs Ag/AgCl in V	ξ in mV
A	83.3 (1.7)	0.21 (1.04)	-1.142 (0.004)	46 (4)
B	21.8 (0.5)	0.27 (0.21)	-1.169 (0.004)	49 (3)
C	5.6 (0.2)	0.31 (0.05)	-1.190 (0.006)	66 (4)

determined. As expected ΔA_2 is near zero because this parameter describes the behavior of the system under the application of small potential amplitudes. The maximum extent of bleaching is different for each transition because they have different absorption cross-sections. It seems logical that intensive transitions produce stronger bleach signals than weaker ones.
A much larger discrepancy of about 20 to 25 mV for the three inflection points can be observed. The broadening parameter (ξ) of the sigmoid curves are comparable to those obtained from the quantum dot experiments. Because of the interpretation of the inflection point as the band edge potential of the e1 band (lowest sub-band in the conduction band) it is expected to be the same for all three values and the reason for this discrepancy is presently under investigation. A possible explanation including a distinction of the e1-band because of its strong geometrical anisotropy in different sub-bands is unlikely as if this were the case, the linear absorption spectrum should show additional transitions which in this study could not be observed. In addition the selection rules are determined only by the parity of the wave function, not by the origin of the electrons (hh- or lh-origin).

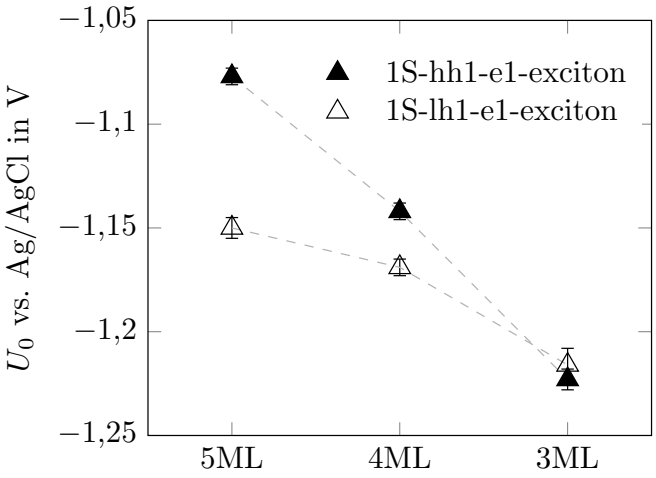

Figure 7: *Evolution of the assumed conduction band edges according to the thickness of the nanoplatelets. The filled triangles denote the potentials that are obtained from analysis of the first exciton of the hh-subband (hh1-exciton). Analog the empty triangles are related to the quenching of the lh1-exciton.*

Size Dependence

Variation of spatial confinement in the z-direction (perpendicular to the particle area) has a major influence on the optical and electronic properties of the platelets. With decreasing thickness the quantization in the z-direction becomes stronger and the energy eigenvalues of the electronic states increase. Thus, the band edges become more separated which leads to the observed blue shift in the fundamental absorption.
Measured EMAS Spectra and corresponding linear absorption spectra are given in the supporting information (Figure S2 for 5 mono layer and Figure S3 for 3 mono layer).
The apparent discrepancy of U_0, depending on the analysis of the hh-exciton on the one hand and of the lh-exciton on the other, indicates that the generation of excitons out of these subbands is affected differently by the application of an external potential. This is a significant difference to the case of the spherical particles. The more profound reason for this observation might be the fact that spherical nanoparticles in the above mentioned size range are more related to discrete molecules than platelets which show bulk-like behavior in two dimensions. The quasi-

continuous sub-bands of the platelet may lead to charging effects which are different from the processes observed in spherical nanoparticles.
In this context it might be helpful to apply EMAS on one-dimensional nanostructures to investigate the influence of continuous regions in the DOS with more certainty. Building on that, a new EMAS model should be sought, that includes

- the density of states, both of the upper valence band and the lower conduction band
- surface states and thus the generation of additional parts of the density of states within the bandgap region
- an insulating barrier between the particles and the conductive electrode due to organic capping ligands and thin oxide layers due to oxidation of the semiconductor nanomaterial[72,73]
- influence of charging effects on the band structure of spherical particles and platelets.

Conclusion

EMAS as a spectroelectrochemical method has been applied successfully to semiconductor nanostructures with the specific aim to identify band edge positions according to a well defined reference electrode. A bleaching model has been derived and its application to the difference spectra yields reproducible band edge energies. Using lock-in amplification extremely weak signal amplitudes are resolvable which allows the investigation of mono- and submonolayers of particles attached to the transparent working electrode.
The investigations have been carried out for spherical CdSe-nanoparticles and CdSe-nanoplatelets. The bleach model fits very well for the spherical particles but there are complications with the more continuous band nature of the platelet structures, which manifest themselves in a discrepancy of the inflection points for different transitions that should in principle be identical. Further measurements are required in order to bring more certainty to the field of anisotropic nanostructures.

Acknowledgement We would like to thank Mrs. Susanne Goldberg for the SEM and TEM measurements.
We gratefully acknowledge the International Excellence Graduate School on Emerging Materials and Processes Korea (iEGSEMP Korea) in the context of TU Dresdens Institutional Strategy The Synergetic University, the Deutsche Forschungsgemeinschaft through grant HI-1113/5-1, the Science Foundation lreland's ETS Walton Visitor award scheme grant 11/W.1/12085 and the European Research Council for the ERC AdG AEROCAT.

Supporting Information Available: The supporting information include a detailed description of the EMAS setup and a specification table. List of chemicals, synthetic procedures, buildup of the measuring cell and further data to which hints in the main article were given are also presented. This material is available free of charge via the Internet at `http://pubs.acs.org/`.

References

1. Kamat, P. V. Meeting the Clean Energy Demand: Nanostructure Architectures for Solar Energy Conversion. *J. Phys. Chem. C* **2007**, *111*, 2834–2860.
2. Bang, J. H.; Kamat, P. V. Solar Cells by Design: Photoelectrochemistry of TiO_2 Nanorod Arrays Decorated with CdSe. *Adv. Funct. Mater.* **2010**, *20*, 1970–1976.
3. Kamat, P. V.; Tvrdy, K.; Baker, D. R.; Radich, J. G. Beyond Photovoltaics: Semiconductor Nanoarchitectures for Liquid-Junction Solar Cells. *Chem. Rev.* **2010**, *110*, 6664–6688.
4. Rühle, S.; Shalom, M.; Zaban, A. Quantum-Dot-Sensitized Solar Cells. *ChemPhysChem* **2010**, *11*, 2290–2304.

5. Otto, T.; Müller, M.; Mundra, P.; Lesnyak, V.; Demir, H. V.; Gaponik, N.; Eychmüller, A. Colloidal Nanocrystals Embedded in Macrocrystals: Robustness, Photostability, and Color Purity. *Nano Lett.* **2012**, *12*, 5348–5354.

6. Dabbousi, B. O.; Bawendi, M. G.; Onitsuka, O.; Rubner, M. F. Electroluminescence from CdSe Quantum-Dot/Polymer Composites. *Appl. Phys. Lett.* **1995**, *66*, 1316–1318.

7. Panda, S. K.; Hickey, S. G.; Demir, H. V.; Eychmüller, A. Bright White-Light Emitting Manganese and Copper Co-Doped ZnSe Quantum Dots. *Angew. Chem., Int. Ed.* **2011**, *50*, 4432–4436.

8. Gaponik, N.; Hickey, S. G.; Dorfs, D.; Rogach, A. L.; Eychmüller, A. Progress in the Light Emission of Colloidal Semiconductor Nanocrystals. *Small* **2010**, *6*, 1364–1378.

9. Trindade, T.; O'Brien, P.; Pickett, N. L. Nanocrystalline Semiconductors: Synthesis, Properties, and Perspectives. *Chem. Mater.* **2001**, *13*, 3843–3858.

10. Watt, A.; Thomsen, E.; Meredith, P.; Rubinsztein-Dunlop, H. A New Approach to the Synthesis of Conjugated Polymer-Nanocrystal Composites for Heterojunction Optoelectronics. *Chem. Commun.* **2004**, 2334–2335.

11. Zheng, Y.; Zheng, L.; Zhan, Y.; Lin, X.; Zheng, Q.; Wei, K. Ag/ZnO Heterostructure Nanocrystals: Synthesis, Characterization, and Photocatalysis. *Inorg. Chem.* **2007**, *46*, 6980–6986.

12. Nagaveni, K.; Sivalingam, G.; Hegde, M. S.; Madras, G. Solar Photocatalytic Degradation of Dyes: High Activity of Combustion Synthesized Nano TiO_2. *Appl. Catal., B* **2004**, *48*, 83–93.

13. Yue, Z.; Lisdat, F.; Parak, W. J.; Hickey, S. G.; Tu, L.; Sabir, N.; Dorfs, D.; Bigall, N. C. Quantum-Dot-Based Photoelectrochemical Sensors for Chemical and Biological Detection. *ACS Appl. Mater. Interfaces* **2013**, *5*, 2800–2814.

14. Yuan, J.; Gaponik, N.; Eychmüller, A. Application of Polymer Quantum Dot-Enzyme Hybrids in the Biosensor Development and Test Paper Fabrication. *Anal. Chem.* **2012**, *84*, 5047–5052.

15. Yuan, J.; Wen, D.; Gaponik, N.; Eychmüller, A. Enzyme-Encapsulating Quantum Dot Hydrogels and Xerogels As Biosensors: Multifunctional Platforms for Both Biocatalysis and Fluorescent Probing. *Angew. Chem., Int. Ed.* **2013**, *125*, 1010–1013.

16. Dubavik, A.; Sezgin, E.; Lesnyak, V.; Gaponik, N.; Schwille, P.; Eychmüller, A. Penetration of Amphiphilic Quantum Dots Through Model and Cellular Plasma Membranes. *ACS Nano* **2012**, *6*, 2150–2156.

17. Colvin, V. L.; Alivisatos, A. P.; Tobin, J. G. Valence-Band Photoemission From a Quantum-Dot System. *Phys. Rev. Lett.* **1991**, *66*, 2786–2789.

18. Chun, W.-J.; Ishikawa, A.; Fujisawa, H.; Takata, T.; Kondo, J. N.; Hara, M.; Kawai, M.; Matsumoto, Y.; Domen, K. Conduction and Valence Band Positions of Ta_2O_5, TaON, and Ta_3N_5 by UPS and Electrochemical Methods. *J. Phys. Chem. B* **2003**, *107*, 1798–1803.

19. Cahen, D.; Kahn, A. Electron Energetics at Surfaces and Interfaces: Concepts and Experiments. *Adv. Mater.* **2003**, *15*, 271–277.

20. van Buuren, T.; Dinh, L. N.; Chase, L. L.; Siekhaus, W. J.; Terminello, L. J. Changes in the Electronic Properties of Si Nanocrystals As a Function of Particle Size. *Phys. Rev. Lett.* **1998**, *80*, 3803–3806.

21. Munro, A. M.; Zacher, B.; Graham, A.; Armstrong, N. R. Photoemission Spectroscopy of Tethered CdSe Nanocrystals: Shifts in Ionization Potential and Local Vacuum Level As a Function of Nanocrystal

Capping Ligand. *ACS Appl. Mater. Interfaces* **2010**, *2*, 863–869.

22. Gomes, W.; Cardon, F. Electron Energy Levels in Semiconductor Electrochemistry. *Prog. Surf. Sci.* **1982**, *12*, 155–215.

23. Beranek, R. (Photo)electrochemical Methods for the Determination of the Band Edge Positions of TiO_2-Based Nanomaterials. *Adv. Phys. Chem.* **2011**, *2011*, 1–20.

24. Houtepen, A. J.; Vanmaekelbergh, D. Orbital Occupation in Electron-Charged CdSe Quantum-Dot Solids. *J. Phys. Chem. B* **2005**, *109*, 19634–19642.

25. Xu, Y.; Schoonen, M. A. The Absolute Energy Positions of Conduction and Valence Bands of Selected Semiconducting Minerals. *Am. Mineral.* **2000**, *85*, 543–556.

26. Nozik, A. J. Photoelectrochemistry: Applications to Solar Energy Conversion. *Annu. Rev. Phys. Chem.* **1978**, *29*, 189–222.

27. Gerischer, H. Neglected Problems in the pH Dependence of the Flatband Potential of Semiconducting Oxides and Semiconductors Covered with Oxide Layers. *Electrochim. Acta* **1989**, *34*, 1005–1009.

28. Miller, E. M.; Kroupa, D. M.; Zhang, J.; Schulz, P.; Marshall, A. R.; Kahn, A.; Lany, S.; Luther, J. M.; Beard, M. C.; Perkins, C. L.; van de Lagemaat, J. Revisiting the Valence and Conduction Band Size Dependence of PbS Quantum Dot Thin Films. *ACS Nano* **2016**, *10*, 3302–3311.

29. Liu, C. Y.; Bard, A. J. A Charge-Induced Absorption-Edge Shift in Cadmium Sulfide Semiconductor Films. *J. Phys. Chem.* **1989**, *93*, 7749–7750.

30. Yu, D.; Wang, C.; Guyot-Sionnest, P. n-Type Conducting CdSe Nanocrystal Solids. *Science* **2003**, *300*, 1277–1280.

31. Rothenberger, G.; Fitzmaurice, D.; Graetzel, M. Spectroscopy of Conduction Band Electrons in Transparent Metal Oxide Semiconductor Films: Optical Determination of the Flatband Potential of Colloidal Titanium Dioxide Films. *J. Phys. Chem.* **1992**, *96*, 5983–5986.

32. Jacobsson, T. J.; Edvinsson, T. Photoelectrochemical Determination of the Absolute Band Edge Positions as a Function of Particle Size for ZnO Quantum Dots. *J. Phys. Chem. C* **2012**, *116*, 15692–15701.

33. Doherty, R. P.; Hickey, S. G.; Riley, D.; Tull, E. J. A Study of CdS Nanoparticle Surface States by Potential-Modulated Sub-Bandgap Spectroscopy. *J. Electroanal. Chem.* **2004**, *569*, 271–274.

34. O'Regan, B.; Graetzel, M.; Fitzmaurice, D. Optical Electrochemistry. 2. Real-Time Spectroscopy of Conduction Band Electrons in a Metal Oxide Semiconductor Electrode. *J. Phys. Chem.* **1991**, *95*, 10525–10528.

35. O'Regan, B.; Grätzel, M.; Fitzmaurice, D. Optical Electrochemistry I: Steady-State Spectroscopy of Conduction-Band Electrons in a Metal Oxide Semiconductor Electrode. *Chem. Phys. Lett.* **1991**, *183*, 89–93.

36. Berger, T.; Anta, J. A.; Morales-Flórez, V. Electrons in the Band Gap: Spectroscopic Characterization of Anatase TiO_2 Nanocrystal Electrodes under Fermi Level Control. *J. Phys. Chem. C* **2012**, *116*, 11444–11455.

37. Hoyer, P.; Weller, H. Potential-Dependent Electron Injection in Nanoporous Colloidal ZnO Films. *J. Phys. Chem.* **1995**, *99*, 14096–14100.

38. Wang, C.; Shim, M.; Guyot-Sionnest, P. Electrochromic Semiconductor Nanocrystal Films. *Appl. Phys. Lett.* **2002**, *80*, 4–6.

39. Guyot-Sionnest, P.; Wang, C. Fast Voltammetric and Electrochromic Response of Semiconductor Nanocrystal Thin Films. *J. Phys. Chem. B* **2003**, *107*, 7355–7359.

40. Wehrenberg, B. L.; Guyot-Sionnest, P. Electron and Hole Injection in PbSe Quantum

Dot Films. *J. Am. Chem. Soc.* **2003**, *125*, 7806–7807.

41. Wehrenberg, B. L.; Yu, D.; Ma, J.; Guyot-Sionnest, P. Conduction in Charged PbSe Nanocrystal Films. *J. Phys. Chem. B* **2005**, *109*, 20192–20199.

42. Boehme, S. C.; Vanmaekelbergh, D.; Evers, W. H.; Siebbeles, L. D. A.; Houtepen, A. J. *In Situ* Spectroelectrochemical Determination of Energy Levels and Energy Level Offsets in Quantum-Dot Heterojunctions. *J. Phys. Chem. C* **2016**, *120*, 5164–5173.

43. Araci, Z. O.; Shallcross, C. R.; Armstrong, N. R.; Saavedra, S. S. Potential-Modulated Attenuated Total Reflectance Characterization of Charge Injection Processes in Monolayer-Tethered CdSe Nanocrystals. *J. Phys. Chem. Lett.* **2010**, *1*, 1900–1905.

44. Hickey, S. G.; Riley, D. Intensity Modulated Photocurrent Spectroscopy Studies of CdS Nanoparticle Modified Electrodes. *Electrochim. Acta* **2000**, *45*, 3277–3282.

45. Bard, A. J.; Faulkner, L. R. Electrochemical Methods: Fundamentals and Applications. In *Wiley*; 2001.

46. Reiss, H. The Fermi Level and the Redox Potential. *J. Phys. Chem.* **1985**, *89*, 3783–3791.

47. Efros, A. L.; Rosen, M.; Kuno, M.; Nirmal, M.; Norris, D. J.; Bawendi, M. Band-Edge Exciton in Quantum Dots of Semiconductors with a Degenerate Valence Band: Dark and Bright Exciton States. *Phys. Rev. B* **1996**, *54*, 4843–4856.

48. Elangovan, E.; Ramamurthi, K. A Study on Low Cost-High Conducting Fluorine and Antimony-Doped Tin Oxide Thin Films. *Appl. Surf. Sci.* **2005**, *249*, 183–196.

49. Wang, J.; Lu, J.; Kirgöz, Ü. A.; Hocevar, S. B.; Ogorevc, B. Insights Into the Anodic Stripping Voltammetric Behavior of Bismuth Film Electrodes. *Anal. Chim. Acta* **2001**, *434*, 29–34.

50. Guyot-Sionnest, P. Charging Colloidal Quantum Dots by Electrochemistry. *Microchim. Acta* **2008**, *160*, 309–314.

51. Shim, M.; Wang, C.; Guyot-Sionnest, P. Charge-Tunable Optical Properties in Colloidal Semiconductor Nanocrystals. *J. Phys. Chem. B* **2001**, *105*, 2369–2373.

52. Colvin, V. L.; Alivisatos, A. P. CdSe Nanocrystals with a Dipole Moment in the First Excited State. *J. Chem. Phys.* **1992**, *97*, 730–733.

53. Colvin, V. L.; Cunningham, K. L.; Alivisatos, a. P. Electric Field Modulation Studies of Optical Absorption in CdSe Nanocrystals: Dipolar Character of the Excited State. *J. Chem. Phys.* **1994**, *101*, 7122–7138.

54. Hache, F.; Ricard, D.; Flytzanis, C. Quantum-Confined Stark Effect in Very Small Semiconductor Crystallites. *Appl. Phys. Lett.* **1989**, *55*, 1504–1506.

55. Sacra, A.; Norris, D. J.; Murray, C. B.; Bawendi, M. G. Stark Spectroscopy of CdSe Nanocrystallites: The Significance of Transition Linewidths. *J. Chem. Phys.* **1995**, *103*, 5236–5245.

56. Norris, D. J.; Sacra, A.; Murray, C. B.; Bawendi, M. G. Measurement of the Size Dependent Hole Spectrum in CdSe Quantum Dots. *Phys. Rev. Lett.* **1994**, *72*, 2612–2615.

57. Woggon, U.; Wind, O.; Gindele, F.; Tsitsishvili, E.; Müller, M. Optical Transitions in CdSe Quantum Dots: From Discrete Levels to Broad Gain Spectra. *J. Lumin.* **1996**, *70*, 269–280.

58. Norris, D. J.; Bawendi, M. G. Measurement and Assignment of the Size-Dependent Optical Spectrum in CdSe Quantum Dots. *Phys. Rev. B* **1996**, *53*, 16338–16346.

59. Ekimov, A. I.; Kudryavtsev, I. A.; Efros, A. L.; Yazeva, T. V.; Hache, F.; Schanne-Klein, M. C.; Rodina, A. V.; Ricard, D.; Flytzanis, C. Absorption and Intensity-Dependent Photoluminescence Measurements on CdSe Quantum Dots: Assignment of the First Electronic Transitions. *J. Opt. Soc. Am. B* **1993**, *10*, 100–107.

60. Park, S. H.; Morgan, R. A.; Hu, Y. Z.; Lindberg, M.; Koch, S. W.; Peyghambarian, N. Nonlinear Optical Properties of Quantum-Confined CdSe Microcrystallites. *J. Opt. Soc. Am. B* **1990**, *7*, 2097–2105.

61. Harris, D. C.; Werner, G. Lehrbuch der Quantitativen Analyse. In *Springer-Verlag*; 2014.

62. Sapra, S.; Sarma, D. D. Evolution of the Electronic Structure with Size in II-VI Semiconductor Nanocrystals. *Phys. Rev. B* **2004**, *69*, 125304.

63. Brus, L. Electronic Wave Functions in Semiconductor Clusters: Experiment and Theory. *J. Phys. Chem.* **1986**, *90*, 2555–2560.

64. Schmidt, H.; Weller, H. Quantum Size Effects in Semiconductor Crystallites: Calculation of the Energy Spectrum for the Confined Exciton. *Chem. Phys. Lett.* **1986**, *129*, 615–618.

65. Nair, S. V.; Ramaniah, L. M.; Rustagi, K. C. Electron States in a Quantum Dot in an Effective-Bond-Orbital Model. *Phys. Rev. B* **1992**, *45*, 5969–5979.

66. Kayanuma, Y.; Momiji, H. Incomplete Confinement of Electrons and Holes in Microcrystals. *Phys. Rev. B* **1990**, *41*, 10261–10263.

67. Sapra, S.; Shanthi, N.; Sarma, D. D. Realistic Tight-Binding Model for the Electronic Structure of II-VI Semiconductors. *Phys. Rev. B* **2002**, *66*, 205202.

68. Puntambekar, A.; Wang, Q.; Miller, L.; Smieszek, N.; Chakrapani, V. Electrochemical Charging of CdSe Quantum Dots: Effects of Adsorption *Versus* Intercalation. *ACS Nano* **2016**, *10*, 10988–10999.

69. Boehme, S. C.; Wang, H.; Siebbeles, L. D. A.; Vanmaekelbergh, D.; Houtepen, A. J. Electrochemical Charging of CdSe Quantum Dot Films: Dependence on Void Size and Counterion Proximity. *ACS Nano* **2013**, *7*, 2500–2508.

70. Achtstein, A. W.; Schliwa, A.; Prudnikau, A.; Hardzei, M.; Artemyev, M. V.; Thomsen, C.; Woggon, U. Electronic Structure and Exciton-Phonon Interaction in Two-Dimensional Colloidal CdSe Nanosheets. *Nano Lett.* **2012**, *12*, 3151–3157.

71. Achtstein, A. W.; Prudnikau, A. V.; Ermolenko, M. V.; Gurinovich, L. I.; Gaponenko, S. V.; Woggon, U.; Baranov, A. V.; Leonov, M. Y.; Rukhlenko, I. D.; Fedorov, A. V.; Artemyev, M. V. Electroabsorption by 0D, 1D, and 2D Nanocrystals: A Comparative Study of CdSe Colloidal Quantum Dots, Nanorods, and Nanoplatelets. *ACS Nano* **2014**, *8*, 7678–7686.

72. Patel, B. K.; Nanda, K. K.; Sahu, S. N. Interface Characterization of Nanocrystalline CdS/Au Junction by Current-Voltage and Capacitance-Voltage Studies. *J. Appl. Phys.* **1999**, *85*, 3666–3670.

73. Kim, S.-H.; Markovich, G.; Rezvani, S.; Choi, S. H.; Wang, K. L.; Heath, J. R. Tunnel Diodes Fabricated from CdSe Nanocrystal Monolayers. *Appl. Phys. Lett.* **1999**, *74*, 317–319.

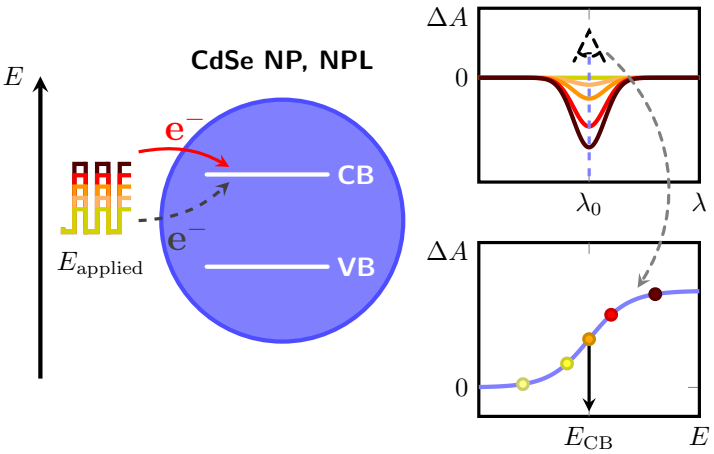
CdSe NP, NPL
E
e⁻
e⁻
CB
VB
E_applied
ΔA
0
λ₀
λ
ΔA
0
E_CB
E